End-winding resonance, should be order or not

EUR23_25

Lucas Selonke Klaas
WEG
Jaragua do Sul
Brazil

Fredemar Runcos
WEG
Jaragua do Sul
Brazil

Fernando Roberto Spezia
WEG
Jaragua do Sul
Brazil

Abstract - During the design stage of an electric motor or generator, the components are evaluated according to the operating loads.

It is important that resonances are removed in relation to the excitation frequencies to avoid amplification of vibration that will increase mechanical loads that could lead to premature fail.

For evaluation of the rotor, lateral and torsional analyses are performed to find the natural frequencies. Similarly, the natural frequencies of the static part are conducted for housing, cover, and stator core.

However, the end-winding has innumerous nonlinearities, multiple types of fastening, different types of materials, and fibers that are dependent on the impregnation process to achieve the correct stiffness to support the coils. In this way, to have precise results, it is necessary to measure the natural frequency of the end-winding. This paper presents the evaluation of natural frequency of end-winding of 50 electrical machines.

Index Terms — End-winding resonance test (EWRT), induction motor, synchronous generator.

I. INTRODUCTION

The focus of the article will be on stator winding. It is important to point out that there are several types of windings when it comes to electrical machines. The most common in the manufacture of electric motors and generators are the coils with circular wires, without a specific format, and the pre-formed coils, as the name implies, have a format according to the electrical project specification. Usually, the circular wire coils are used in machines with lower power, while the pre-shaped coils are used in larger machines. This analysis is performed to large machines with form-wound winding.

Besides the type of end-winding, due to the length and diameter, it is common for form-wound winding the addition of support on the pressing ring of the stator to hold the end-winding to withstand the high electromagnetic force loading when the machine has an electrical fault, but also increase the natural frequency of the system. The supports vary according to the manufacturer but in general, are plates and rings. The materials of these supports usually are steel which is not in contact with the winding directly, the materials that connect the winding and steel are glass fiber, cords, and bandings.

Due to the factors previously mentioned in the abstract, numerical modal analysis is not a simple task to employ, thus the use of experimental modal analysis (EMA) of stator end-windings is necessary. Although the modal analysis is a measurement employed in many industries it is not so commonly applied in electronics manufacturing. Therefore, the introduction of the standard IEC 60034-32:2016 presents standardization for this type of test, both in the preparation, execution, and evaluation of results.

For a complete evaluation of the end-winding and to understand the customer's real need for the test request. The paper is divided into six parts. In the second part, a theoretical analysis of the excitation forces on the end-winding and the vibration analysis is performed. In the third part, the measurement procedure is presented. In the fourth, the experimental results are presented. Then, in the fifth part, the end-winding failure cases are presented. Finally, in the conclusion with the evaluation of the measurements.

The summary of measured machines is in the plots that present the relation of quantity and number of poles (Figure 1), quantity and frame size (Figure 2), and power and frame size (Figure 3).

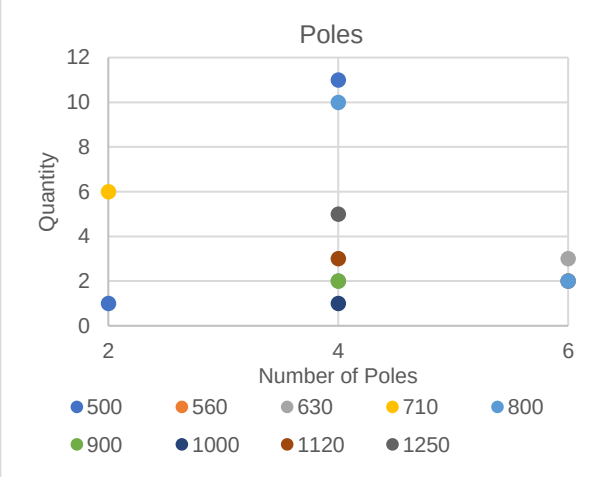

Figure 1 – Quantity of machines per polarity.

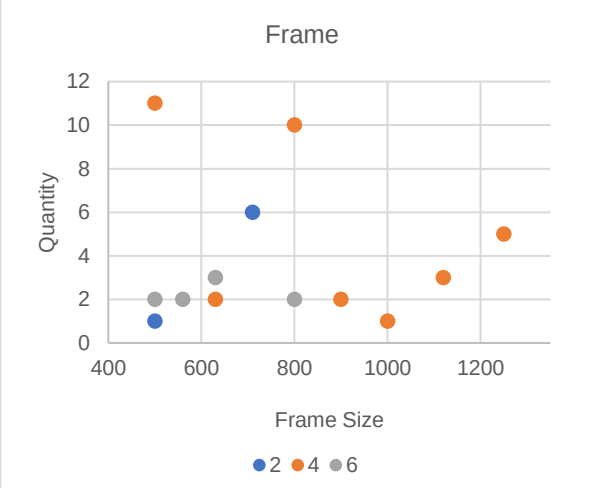

Figure 2 – Quantity of machines per frame size.

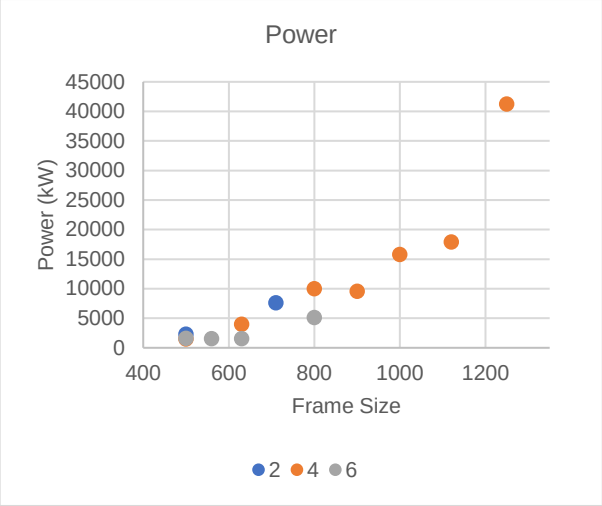

Figure 3 – Power per frame size.

II. EXCITATION FORCES ON THE END-WINDING

The analysis of efforts in the end-winding of the three-phase electric machine is not a simple task. The complexity lies in the spatial geometry of the distribution of conductors in the region of the end-winding.

It is known that when in each region of space an electric current density circulates $\vec{J}$ around the current density vector the magnetic induction vector circulates $\vec{B}$ defined by Ampere's law:

$$\oint_C \vec{B} \cdot d\vec{l} = \mu_0 \cdot \iint_S \vec{J} \cdot d\vec{S} \qquad (2.1)$$

In equation (2.1) the vector $\vec{B}$ now represents the magnetic induction vector given in [T], the vector $d\vec{l}$ represents an element of length given in [m], the vector $\vec{J}$ represents the electric current density vector given in [A/m^2]. The vector $d\vec{S}$ represents the cross section in the region of space through which the current density circulates. In the space region of the end-winding we have air where the magnetic permeability assumes the value $\mu_0 = 4\pi \times 10^{-7}$[Tm/A].

To carry out a quantitative analysis of the efforts in the conductors of the end-winding, it is necessary to determine the magnetic induction vector $\vec{B}$ at all points in the space occupied by the conductors. This solution is difficult, and it is not possible to solve it analytically due to the complexity of the spatial geometry of the conductors in the region occupied by the end-winding. A quantitative analysis with a good deal of accuracy can be obtained through a three-dimensional modeling of the end-winding in finite elements. However, this analysis takes time and is not always possible.

Due to the complexity of the problem, a qualitative analysis of the behavior of the end-winding is usually carried out when subjected to electromagnetic forces arising from the operating condition in the steady state and transient state of the machine. This qualitative analysis can be done in a very objective way using the Lorentz electromagnetic force law.

For this analysis we will use the reference system in cylindrical coordinates illustrated in Figure 4.

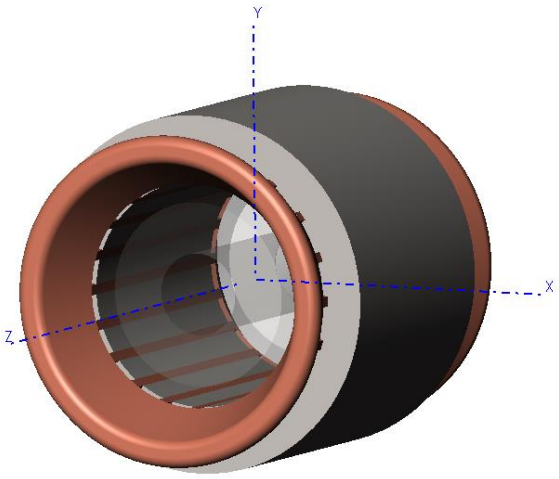

Figure 4 - Cylindrical coordinate system to position the end-winding.

The conductors of the three phases in the spatial region occupied by the end-winding obey the same linear distribution of the conductors housed inside the slots. This linear distribution of the conductors is offset in the azimuthal direction in relation to that of the conductors inside the slots due to the geometry of the coils in the region occupied by the end-windings. This lag is a function of the axial z coordinate of the coordinate system. The current of each phase circulating through the linear distribution of conductors of each phase generates a pulsating wave of linear density of electric current per phase that are lagged in time and space of $(2\pi/3)$ electric radians. The sum in space of the three pulsating waves of linear density of electric current forms a wave of linear density of resulting current $\vec{J}_{\nu_{L1}}(\rho, \phi, z, t)$, given that [A/m] it goes in the azimuthal direction in the space occupied by the end-winding.

It can be shown that the wave resulting from the current linear density $\vec{J}_{\nu_{L1}}(\rho, \phi, z, t)$ for an order ν_{L1} harmonic is given by:

$$\vec{J}_{\nu_{L1}}(\rho_1, \phi_1, z_1, t) = \left[A_{J_{\nu_{L1}}} \cdot e^{j\cdot(\nu_{L1}\cdot\phi_1 - \omega_{\nu_{L1}}\cdot t - \varphi_{\nu_{L1}})}\right] \vec{r}_{uj} \qquad (2.2)$$

The vector $\vec{r}_{uj}$ in equation (2.2) represents the unit vector indicating the direction of the vector $\vec{J}_{\nu_{L1}}(\rho, \phi, z, t)$ at the point in the space of the end-winding where the loads are to be analyzed.

The amplitude $A_{J_{\nu_{L1}}}$ of the linear current density wave in equation (2.2) is a function of the number of coil conductors, the current flowing through the coil conductors, and the coordinates of the point in the space occupied by the end-winding (ρ_1, ϕ_1, z_1, t) where we want to analyze the efforts.

The harmonic order ν_{L1} of the linear density of electric current, in number of pairs of poles of the machine, as it is a spatial distribution of the conductors of a three-phase winding, is given by:

$$\nu_{L1} = p \cdot \left[1 + g_{L1} \cdot \left(\frac{2 \cdot m_1}{c_1}\right)\right] \qquad (2.3)$$

In equation (2.3) p represents the number of pairs of poles of the machine, m_1 represents the number of phases and c_1 represents the fractional part of the winding, for whole $c_1 = 1.0$ winding. The term g_{L1} in equation (2.3) represents an integer number given by:

$$g_{L1} = 0; \pm 1; \pm 2; \pm 3; \pm 4; \pm ..... \quad (2.4)$$

The frequency of the linear current density waves $\omega_{\nu_{L1}}$ in equation (2.2) corresponds to the frequency of the current flowing in the coil conductors, that is:

$$\omega_{\nu_{L1}} = 2 \cdot \pi \cdot f_{line} \quad (2.5)$$

The term $\varphi_{\nu_{L1}}$ represents the initial phase of the linear current density wave that is related to the spatial distribution of the conductors in the end-winding.

Given $[T]$ induction waves $\vec{b}_{\nu_{b1}}(\rho, \phi, z, t)$ which can be generically written as:

$$\vec{b}_{\nu_{b1}}(\rho_1, \phi_1, z_1, t) = \left[B_{\nu_{b1}} \cdot e^{j\cdot\left(\nu_{b1}\cdot\phi_1 - \omega_{\nu_{b1}}\cdot t - \varphi_{\nu_{b1}}\right)}\right]\vec{r}_{ub} \quad (2.6)$$

The vector $\vec{r}_{ub}$ in equation (2.6) represents the unit vector indicating the direction of the vector $\vec{b}_{\nu_{b1}}(\rho, \phi, z, t)$ at the point in the space of the end-winding where the efforts are to be analyzed.

The amplitude $B_{\nu_{b1}}$ of the induction wave in equation (2.6) is a function of the linear current density and the magnetic path permeance of the magnetic field lines of force.

The order of the ν_{b1} induction harmonics, in equation (2.6), in number of pairs of poles of the machine, is the same as the linear current density wave, that is:

$$\nu_{b1} = \nu_{L1} = p \cdot \left[1 + g_{L1} \cdot \left(\frac{2 \cdot m_1}{c_1}\right)\right] \quad (2.7)$$

The frequency of the induction waves $\omega_{\nu_{b1}}$ in equation (2.6) also corresponds to the frequency of the current linear density wave, that is:

$$\omega_{\nu_{b1}} = \omega_{\nu_{L1}} = 2 \cdot \pi \cdot f_{line} \quad (2.8)$$

The term $\varphi_{\nu_{b1}}$ represents the initial phase of the induction wave which is related to the initial phase of the linear current density wave and to the geometry of the magnetic path of the magnetic field lines of force.

Figure 5 illustrates end-winding where the linear density vector of electric current is shown at a given point $\vec{J}_{\nu_{L1}}(\rho, \phi, z, t)$ and the magnetic induction vector at the same point $\vec{b}_{\nu_{b1}}(\rho, \phi, z, t)$.

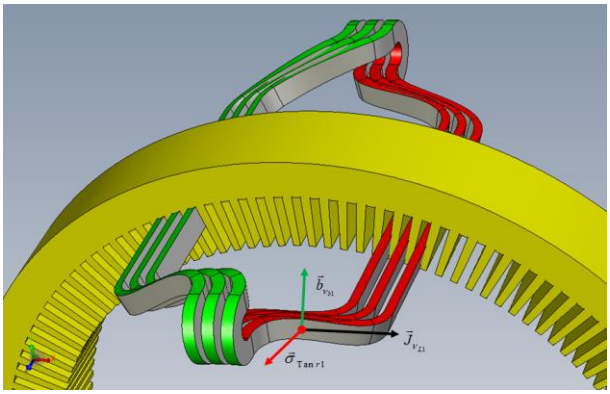

Figure 5 - Electromagnetic force wave at end-winding.

The interaction between the linear current density wave $\vec{J}_{\nu_{L1}}(\rho, \phi, z, t)$ and the induction wave gives the $\vec{b}_{\nu_{b1}}(\rho, \phi, z, t)$ tangential force surface $\vec{\sigma}_{Tan\,r1}(\rho_1, \phi_1, z_1, t)$ density wave. Figure 5 illustrates the three vectors.

For the calculation of density waves of tangential forces $\vec{\sigma}_{Tan\,r1}(\rho_1, \phi_1, z_1, t)$ we will apply the law of Lorentz forces. Applying Lorentz's law to the surface density wave of tangential force $\vec{\sigma}_{Tan\,r1}(\rho_1, \phi_1, z_1, t)$ in [N/m^2], is given by:

$$\vec{\sigma}_{Tan\,r1}(\rho_1, \phi_1, z_1, t) = \left[\vec{J}_{\nu_{L1}}(\rho_1, \phi_1, z_1, t) \times \vec{b}_{\nu_{b1}}(\rho_1, \phi_1, z_1, t)\right]\vec{r}_{u\sigma} \quad (2.9)$$

The vector $\vec{r}_{u\sigma}$ in equation (2.6) represents the unit vector indicating the direction of the vector $\vec{\sigma}_{Tan\,r1}(\rho, \phi, z, t)$ at the point in the space of the end-winding where the efforts are to be analyzed. The force wave given by equation (2.9) is a point function of the space occupied by the end-winding and can have components in the three spatial directions, that is, in the radial x and y direction and in the axial z direction.

Therefore, the magnitude of the density of tangential forces $\sigma_{\mathrm{Tan_{r1}}}(\rho_1, \phi_1, z_1, t)$, considering only the real part of the induction wave, can be generically written as:

$$\sigma_{\mathrm{Tan_{r1}}}(\rho_1, \phi_1, z_1, t) = \frac{1}{2} J_{\nu_{L1}}(\rho_1, \phi_1, z_1, t) \cdot \left[b_{\nu_{b1}}(\rho_1, \phi_1, z_1, t) + b_{\nu_{b1}}(\rho_1, \phi_1, z_1, t) *\right] \quad (2.10)$$

Where $b_{\nu_{b1}}(\rho_1, \phi_1, z_1, t) *$ represents the complex conjugate wave of the induction wave. The tangential force density $\sigma_{\mathrm{Tan_{r1}}}(\rho_1, \phi_1, z_1, t)$ is expressed in (N/m^2) and therefore represents a tangential pressure.

Substituting the induction wave given by (2.6) and the linear current density wave given by equation (2.2) in equation (2.10), we obtain, for each harmonic, two waves of tangential forces given in general by:

$$\sigma_{\mathrm{Tan_{r1}}}(\rho_1, \phi_1, z_1, t) = F_{\mathrm{Tan_{r1}}} \cdot e^{j(\mathrm{r1}\cdot\phi_1 - \omega_{\mathrm{r1}}\cdot t - \varphi_{\mathrm{r1}})} \quad (2.11)$$

In equation (2.11) $F_{\mathrm{Tan_{r1}}}$ represents the amplitude of the tangential force density wave given by:

$$F_{\mathrm{Tan_{r1}}} = \frac{1}{2} A_{J_{\nu_{L1}}} \cdot B_{\nu_{b1}} \quad (2.12)$$

The term r1 in equation (2.11) represents the force wave order, which corresponds to the excitation mode of the tangential force density wave given by:

$$\text{r1} = \nu_{L1} \pm \nu_{b1} \tag{2.13}$$

The angular frequency of the tangential force density wave ω_{r1} is given by:

$$\omega_{\text{r1}} = \omega_{\nu_{L1}} \pm \omega_{\nu_{b1}} \tag{2.14}$$

As the frequency of the induction wave and the linear current density wave are equal and given by equation (2.8), the frequency of the force wave assumes:

$$\omega_{\text{r1}} = \begin{cases} 0 \\ 2 \cdot (2 \cdot \pi \cdot f_{line}) \end{cases} \tag{2.15}$$

The phase constant of the tangential force density wave φ_{r1} is given by:

$$\varphi_{\text{r1}} = \varphi_{\nu_{L1}} \pm \varphi_{\nu_{b1}} \tag{2.16}$$

Equation (2.11) represents two tangential force density waves acting on the surface that passes through the point where the force is to be analyzed, one with an angular ω_{r1} frequency given by the sum and another with an angular ω_{r1} frequency given by the difference of the frequencies of the source waves. Note that the waves result from the interaction of an induction wave and a linear current density wave. The value of the tangential force surface density wave depends on the position (ρ, ϕ_1, z) and time t.

As the induction waves and linear current density waves, in the end-winding region, present the same order for their respective harmonics, the excitation modes given by equation (2.13) present the following pairs of poles:

$$\text{r1} = 0p; \pm 1p; \pm 2p; \pm 3p; \pm 4p; \pm 5p; \pm 6p; \pm 7p.. \tag{2.17}$$

When the machine is manufactured with an integer winding where the term $c_1 = 1$ in equation (2.7) does not present the excitation modes of odd order. Figure 6 illustrates the first excitation modes for a 2-pole machine with $c_1 = 1$.

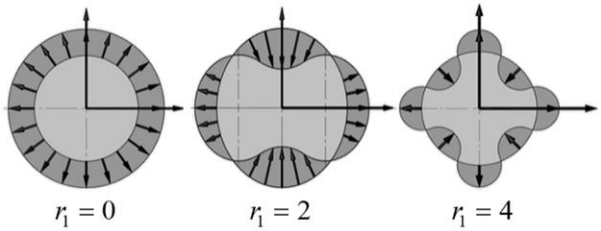

Figure 6 – Excitation modes of tangential electromagnetic force waves.

The surface density of the total tangential force $\sigma_{T_{\text{Total}}}(\rho_1, \varphi_1, z_1, t)$ at the position (ρ_1, ϕ_1, z_1) and time t at the end-winding is obtained by adding the densities of forces generated by the set of harmonics r1, that is:

$$\sigma_{T_{\text{Total}}}(\rho_1, \phi_1, z_1, t) = \sum_{\text{r1}} F_{\text{Tan r1}} \cdot e^{j(\text{r1} \cdot \phi_1 - \omega_{\text{r1}} \cdot t - \varphi_{\text{r1}})} \tag{2.18}$$

Considering the conductors uniformly distributed in the space occupied by the end-winding and the medium occupied by the end-winding isotropic, the elementary tangential force $df_{\text{Tanr}_t}(\rho_1, \phi_1, z_1, t)$ in (N) generated over an area element $dS = \rho_1 \cdot d\phi_1 \cdot dz_1$, by the tangential force density wave $\vec{\sigma}_{Tan\,r1}(\rho_1, \phi_1, z_1, t)$ obtained from equation (2.11) can be written as:

$$\begin{aligned} df_{\text{Tanr}_t}(\rho_1, \phi_1, z_1, t) &= \vec{\sigma}_{Tan\,r1}(\rho_1, \phi_1, z_1, t) \cdot dS \\ &= \left(F_{\text{Tan r1}} \cdot e^{j(\text{r1} \cdot \phi_1 - \omega_{\text{r1}} \cdot t - \varphi_{\text{r1}})}\right) \\ &\quad \cdot (\rho_1 \cdot d\phi_1 \cdot dz_1) \end{aligned} \tag{2.19}$$

The term ρ_1 represents the mean radius of the end-winding at the point where you want to calculate the force on the area element.

The force $df_{\text{Tanr}_t}(\rho_1, \phi_1, z_1, t)$ given by equation (2.19) acts on the circumferential section of the distribution of conductors in the end-winding that per unit length (N/m) can be written as:

$$\begin{aligned} \frac{df_{\text{Tanr}_t}(\rho_1, \phi_1, z_1, t)}{\rho_1 \cdot d\phi_1} &= F_{\text{Ele winding}} \\ &\quad \cdot e^{j(\text{r1} \cdot \phi_1 - \omega_{\text{r1}} \cdot t - \varphi_{\text{r1}})} \end{aligned} \tag{2.20}$$

The force per unit length of equation (2.20) analytically describes the electromagnetic force on (N/m) the end-winding conductors and can be used to analyze the modes of vibration of the end-winding, both in the steady state and in the transient state.

The force wave given by equation (2.20) moves in the azimuthal direction with an angular velocity m (rad/s) given by:

$$\omega_{\text{Force}} = \frac{d}{dt}(r1 \cdot \phi_1 - \omega_{\text{r1}} \cdot t - \varphi_{\text{r1}}) = \frac{\omega_{\text{r1}}}{r1} \tag{2.21}$$

Figure 7 illustrates the electromagnetic force developed in the end-winding for a 2-pole machine and for excitation mode r1 = 2p = 2 at instant of time t.

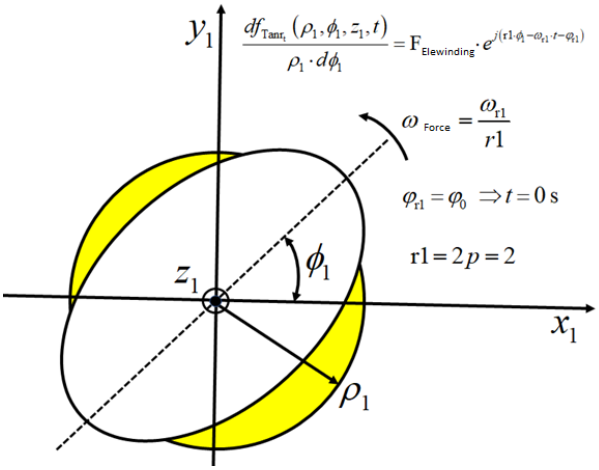

Figure 7 – Electromagnetic force on the end-winding of a 2-pole machine.

In steady-state and transient operation, the force waves given by equation (2.20) act on the structure of the machine's end-winding, producing vibrations. The structure of the end-winding must be properly dimensioned so that these vibrations do not harm the structure during the

operation of the electric machine.

The end-winding structure, despite being complex, presents natural modes of vibration that can be excited by the force waves given by equation (2.20).

Figure 8 illustrates the first natural modes of end-winding vibration, where the most sensitive is the mode $r_n = 2$ because it is normally excited by the 2-pole machine.

Analyzing the results of a detailed modal analysis, the resonance condition does not always lead to an excessive vibration of the end-winding structure. The amplitude of the deflection depends on the structural characteristics, but mainly on the damping of the structural elements.

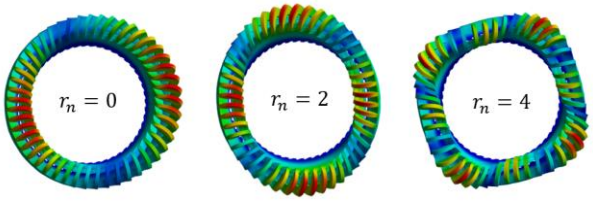

Figure 8 – Natural modes of vibration of the end winding structure significant for 2 and 4 poles.

$$x(\rho_1, \phi_1, z_1, t) = \frac{X_0(\rho_1, \phi_1, z_1, t)}{\sqrt{\left[1 - \left(\frac{\omega_{r1}}{\omega_n}\right)^2\right]^2 + \left[2 \cdot \left(\frac{c}{c_{critical}}\right)\left(\frac{\omega_{r1}}{\omega_n}\right)\right]^2}} \quad (2.22)$$

In equation (2.22) we have:

$X_0(\rho_1, \phi_1, z_1, t)$ is the amplitude of the static deformation of the structure at the point considered.

ω_{r1} is the frequency of the excitation mode of the force.

$c_{critical}$ is the critical damping coefficient of the structure at the considered point.

c is the damping coefficient of the structure at the considered point.

Equation (2.22) shows that when close to a resonance condition $\omega_{r1} \cong \omega_n$ the vibration amplitude can be low depending on the damping of the structure.

When the electromagnetic force waves given by equation (2.20) act on the end-winding elements, the deflection wave $x(\rho_1, \phi_1, z_1, t)$ follows the force with a certain delay. Considering the structure of the isotropic end-winding, the deflection wave can be measured with vibration sensors positioned on the circumference that passes through the point of the end-winding where the modal analysis is to be performed. The deflection wave $x_{r1}(\rho_1, \phi_1, z_1, t)$ can be written as:

$$x_{r1}(\rho_1, \phi_1, z_1, t) = X_{Bobr1} \cdot e^{j\cdot[r1\cdot\phi_1 - \omega_{r1}\cdot t - (\varphi_{r1}+\varphi_{Dynr1})]} \quad (2.23)$$

In equation (2.23) we have:

The term $X_{r1}(\rho_1, \phi_1, z_1, t)$ in equation (2.23) represents the maximum amplitude of deformation of the structure at the considered point caused by the order force wave r1.

The term φ_{Dynr1} in equation (2.23) represents the delay in radians of the strain wave caused by the order force wave r1.

The total deformation $x_{Total}(\rho_1, \phi_1, z_1, t)$ is the best point of the end-winding to measure the modal analysis generated by the waves of electromagnetic force of order r1 is given by:

$$x_{Total}(\rho_1, \phi_1, z_1, t) = \sum_{r1} X_{Bobr1} \cdot e^{j\cdot[r1\cdot\phi_1 - \omega_{r1}\cdot t - (\varphi_{r1}+\varphi_{Dynr1})]} \quad (2.24)$$

Figure 9 illustrates the electromagnetic force developed in the end-winding for a 2-pole machine and the corresponding resulting strain wave for the excitation mode $r1 = 2p = 2$ at instant of time t.

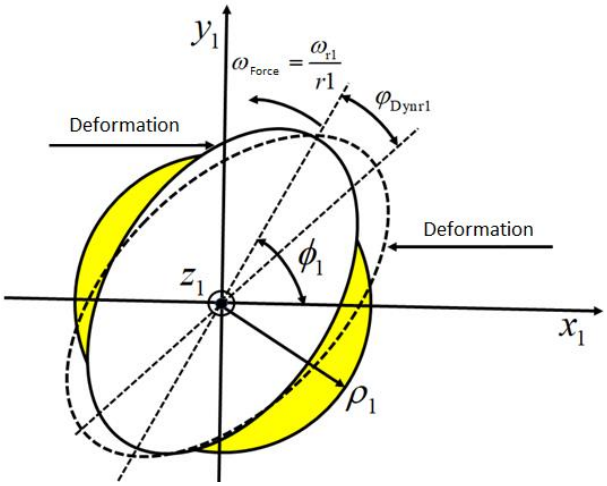

Figure 9 – Electromagnetic force deformation on the end-winding of 2-pole machine.

III. MEASUREMENT PROCEDURE

The procedure includes two different methods depending on the natural frequency of end-winding. Generally, for small machines the natural frequency is much higher in relation to running frequency and two times the line frequency (2xLF). In this case, it is not important to evaluate the mode shape of the end-winding, the safety margin is enough to approve the EWRT.

The main method applied for measurement is the frequency response function (FRF), which are obtained for processing signs acquired from excitations and from responses from structure. For measurement of FRF is applied an instrumented impacting hammer. The attribution of experimental modal analysis are the mode shapes.

The second method is simplest as compared to the main, it is called bump test and it involves the measurement of impact of not instrument hammer and it can be employed not only for end-winding but for several types of components.

A. Experimental Modal Analysis

The dynamic signal analyzer is multichannel frequency for measuring and storing the signal. It is applied two channels, one for the hammer and other for uniaxial transducer. The hammer impacts in the same location, radial direction, for acquisition of FRF and it is used a roving transducer.

The position of impact and measurement is placed in a plane close to the end, distant for stator core. In this plane, the measuring points are equally distance totaling 12 points, that can identify the mode until 11 nodes, in this way it fits for 02 (04-node) and 04 poles (08-node).

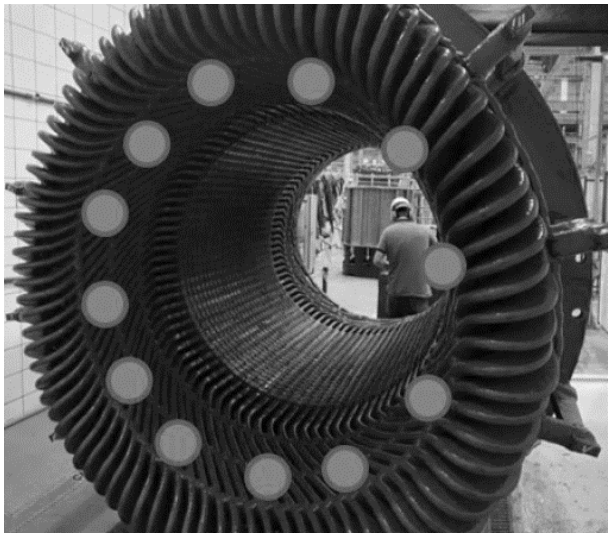

Figure 10 – Example of measuring points for EMA.

The sensors should be installed just before starting the curvature of the winding, so the local in which the response by the impact is higher. The installation of the sensor uses beeswax to ensure a proper fixation to the structure to avoid noise to the measurement. The winding needs to be cleaned to prevent dust that reduces the fixation of the sensor. The sensor has a reduced size in comparison to the regular applied to vibration monitoring, this size is necessary to sit flat on the mounting surface of the selected winding.

1) *Configuration of data acquisition*

The measuring frequency range is 10 Hz to 400 Hz.
Minimum frequency spectrum resolution 0.5 Hz/line

2) *Impact hammer*

Height head 1.34 kg
Soft tip

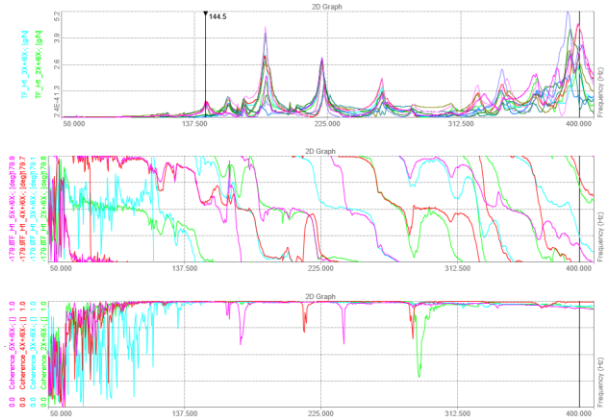

Figure 11 – Example of the sun of FRF in EWRT.

The Figure 11 presents an example of the transfer function (on the top), phase (middle) and the coherence (bottom) of the twelve points. The cursor is placed at 172.4 Hz that correspond to the 04-node mode. It is expected coherence over 70%.

B. Bump Test

The same dynamic signal analyzer used for EMA could also be used for bump test, but it is not mandatory having two channels, only need one channel for transducer, so could be employed a neoprene hammer with 500 grams.

Instead of resulting in modal shapes, the result will be only a spectrum fft with the natural frequencies (peaks). This method could only be employed to check the safety margin from the excitation to the natural frequency.

The configuration of data acquisition should be the same for EMA. The bump is performed in four points spaced 90° from each other. For each measuring point should be performed three bump tests to avoid any measurement errors. At Figure 12 show the first natural frequency at 151 Hz. There is enough safety margin from 2xLF (100 or 120 Hz).

The mounting position of transducer is 180° in reference to the bump as shown at Figure 13.

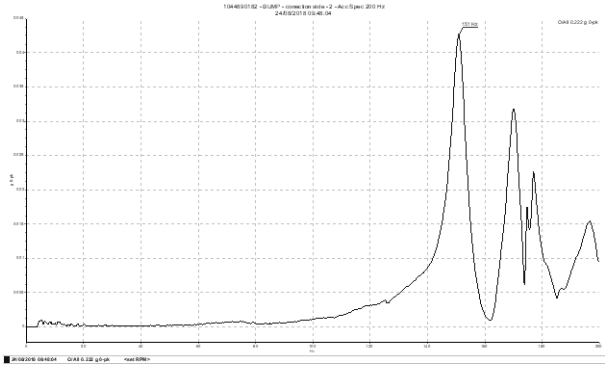

Figure 12 – Spectrum fft measured by bump test.

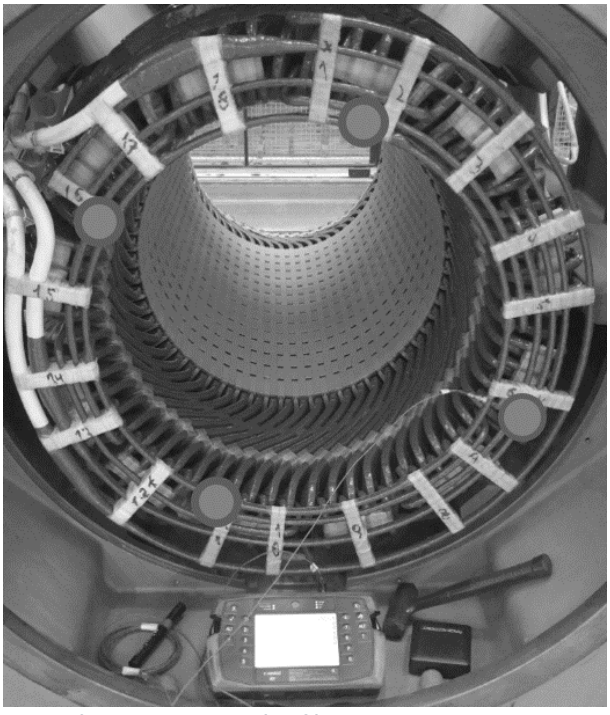

Figure 13 – Example of bump test measurement.

IV. EXPERIMENTAL RESULTS

The natural frequencies presented below is the average between connection side and opposite connection side. The connection side due to the mass of the cables and copper bars that connect the windings presents lower

natural frequency in comparison to the opposite side. When the measurement is performed to a set of machines is informed the average of the set. Even though, each side is evaluated individually in relation to the approval criteria.

A. Approval Criteria

Before establishing an approval criterion, the safety margin will be from the excitation frequency in relation to the mode of interest. It is important to present the concept of global and local vibration mode. The global vibration mode involves the most part of stator end-winding, in order words correspond to a mode that movement the most amount of the mass of structure, in the opposite, the local vibration mode involves small parts of the stator end-winding as individual coil.

Relating to EMA, the safety margin of 15% to 2xLF related to the global mode vibration specific for each polarity. The Figure 14 represents the mode shape harmful to 02 poles, Figure 15 for four poles and Figure 16 for six poles; and 15% to the operating speed frequency (1x) for the mode shape of rigid body in which the end-winding swing in relation to the stator core without present significant local deformation.

Regarding the bump test, there is no information of the mode shape. It is applied the same criterion for EMA but for any natural frequency. In case of failure of approval criteria by the bump test, it should the substituted by EMA.

If the end-winding failures in EMA, there are two options: 1) reinforce the end-winding to increase the frequency of the mode shape or 2) perform the end-winding vibration measurement at the laboratory test. These two actions are not the target of this paper.

B. 02 poles

The total of 50 machines, 07 of them were 02 poles: 01 in frame 500 mm and 06 in frame 710 mm. The natural frequencies are 182 Hz and 162 Hz, respectively. These machines present large safety margin from 2xLF.

Every machine and end-winding has own peculiarities by design as number of slots of stator, voltage, number of connection cables, type of connection (star or delta). These characteristics influences directly on the mass and stiffness of end-winding that are the factors of the natural frequency. Through the tendency line, for two poles, on frame size 1000 mm the safety margin for 2xLF should be lower than 15%. However, generally above the frame size 1000 mm, most of the machines are generators and it has a different concept about the design been called as turbo generators.

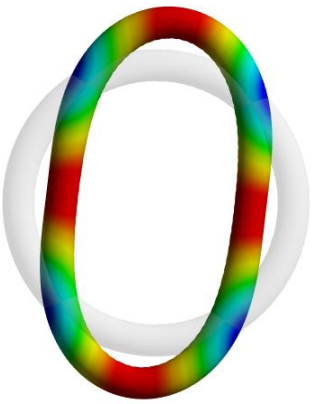

Figure 14 - 04-node mode.

C. 04 poles

The sampling for 04 poles has a total of 34 machines from frame size 500 to 1,250 mm and power from 1,500 kW to 41,250 kVA. In the range of analysis all machines are approved by the criteria with the safety margin above 15%. The lower natural frequency was measured at frame size 1120 and power 17,900 kW.

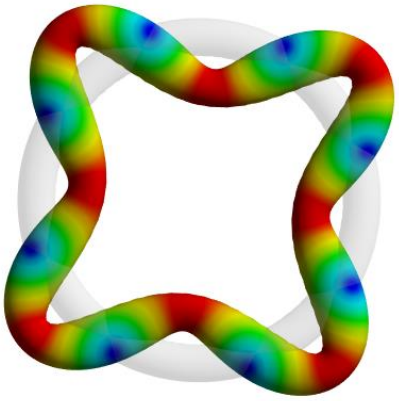

Figure 15 – 08-node mode.

D. 06 poles

The sampling for 06 poles has a total of 09 machines. The number of measuring points of EMA is no adequate to identify the 12-node mode (Figure 17) or higher. For the 06 poles, all machines presented the 12-node mode above the measuring range of 400 Hz, the plot of Figure 16 present the 4-node mode only for verify how far from 2xLF the 12-node could be. The maximum mode found on the measuring range were 10-node.

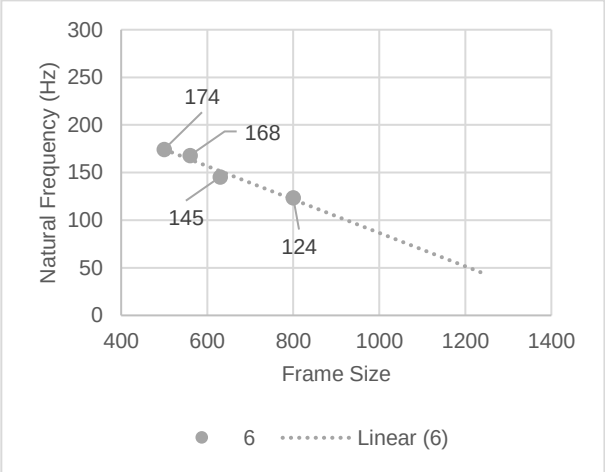

Figure 16 – Natural frequency of 4-node per frame size for 06 poles.

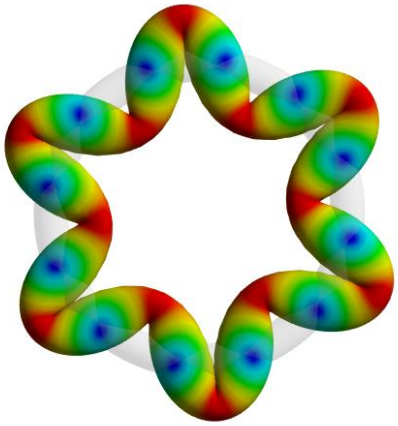

Figure 17 – 12-node mode.

V. EXAMPLES OF END-WINDING FAILURE

The insulation system of rotating electrical machines is frequently exposed to mechanical stresses. Part of this stress is inherent to the service condition of each particular machine, but other parts of it can exist only during the transportation, or only during situations of transient, for example. This paper keeps the focus on the areas of the stator windings out of the slots, the end-windings, not comprising the slot section of the winding, even they can also suffer with mechanical stresses in a significant manner. Other components of the machine, that not the main stator, are also not comprised herein. Stators impregnated in the Global VPI process are the core of this work, no matter motors or generators.

Intrinsic mechanical stresses are intended to be withstood by the insulation system. It means they are known and foreseen on the design of the machines, and will not affect the service life of the insulation, neither the long-term reliability of the machine. Examples are:

- Mechanical vibration of the entire machine;
- Electromagnetic forces;
    - Standstill service condition;
    - Direct-on-line starts (DOL);
    - Synchronization with the power grid;
    - Known and foreseen transients.

Extrinsic mechanical stresses are unexpected, non-specified or unforeseen situations, which can lead to abnormal mechanical stresses acting over the insulation system. Such situations can lead to premature insulation failures or loss of the long-term reliability of the machine. Examples are:

- Collisions or impacts during the transportation and handling;
- Collisions during the assemble of the rotor, turbines, air baffles, etc.;
- Earthquakes, explosions or events that can shake the base were the motor is installed on.
- Sudden rotor blocking or reversion of rotating direction;
- Synchronizations significantly out of the proper phase angle;
- Short circuits on the power line;
- Improper reconnection of a machine still rotating by inertia;
- Excessive hot DOL starts.

Some of the failure mechanisms, which can develop due to mechanical stresses, are described below. The comprehension of the failure mechanisms becomes necessary, to support properly the design and manufacturing processes, which will avoid intrinsic mechanical stresses to become an overstress for the insulation system, leading it to fail prematurely.

The diagram presented below supports the comprehension of the several ageing mechanisms that can take place, due to the mechanical vibration of the end-windings. In any case, an acceleration of the normal ageing behavior of the insulation shall be triggered only in two scenarios: 1) the stress is considered abnormal and the stator is not suitable to withstand it; 2) for any reason, the stator should be suitable to certain stress, but it is not.

Examples of non-rare failure mechanisms are described below, which can be triggered by an unforeseen vibration of the end-windings:

a) Repetitive motion of connections or cable leads, if excessive, can develop cracks on the copper conductors. Consequently, hot spots will develop, extremely overheating the insulation and forcing an electrical breakdown. The loss of continuity, if not leading to a spot electrical breakdown, can force other parts of the winding to work overloaded, imposing higher thermal stress to the insulation and leading to its accelerated ageing. The thermal ageing can develop internal partial discharge activity, which can accelerate the electrical ageing of the insulation.

b) The repetitive motion of the coils on the end-windings, if excessive, can develop cracks on the groundwall insulation, allowing water ingress or developing and electrical treeing. Alternatively, the insulation between turns can be exposed to shearing forces and abrasion. Such mechanical stresses can develop an electrical breakdown to ground or, in case of a preliminary turn fault, can overheat the groundwall insulation extremely before it fails to ground.

c) Excessive motion of the end-windings can also lead to looseness on the bracing system. Lashings can become loose, small gaps can develop between surfaces and intense partial discharge activity can develop. This failure mechanism tends to be slow, if compared to others, but can lead to an electrical breakdown if not ceased on time.

d) Partial discharges are also expected to develop on the slots exists in case the coils can move and crack the interface of the slot corona protection with the slots. Such partial discharges activity can cause the slot corona protection to erode, interrupting the electrical connection with the grading (end corona protection). An electrical breakdown ten to develop, close to the slots, on the coils installed closer to the high voltage side of the phases.

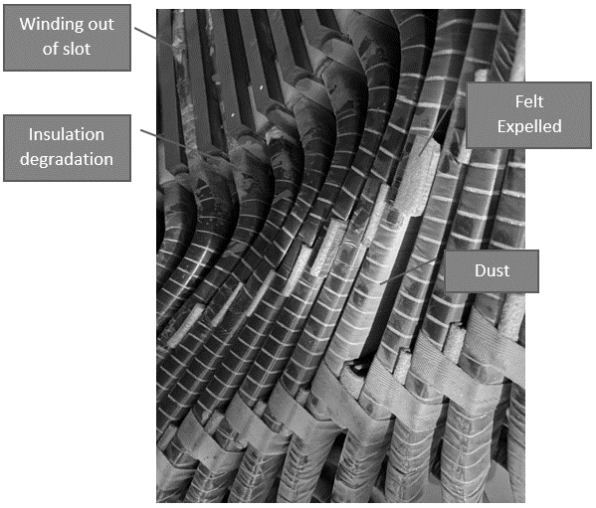

Figure 18 – End-winding failure.

VI. CONCLUSION

The most important cause of generator failure is the stator end-winding vibration [1] according to Insurance Industry. The resulting costs for operating failure and repair represent a minimal percentage of the cost of the test. To avoid amplification of vibration the EWRT is important but according to experimental results no need to be applied in all machines evaluated on this paper.

For six-pole machines do not need to be order the EWRT until frame size 1250 mm. The 12-node mode shape is above 400 Hz for frame size 800 mm, and it will above 2xLF plus safety margin until frame 1250 mm.

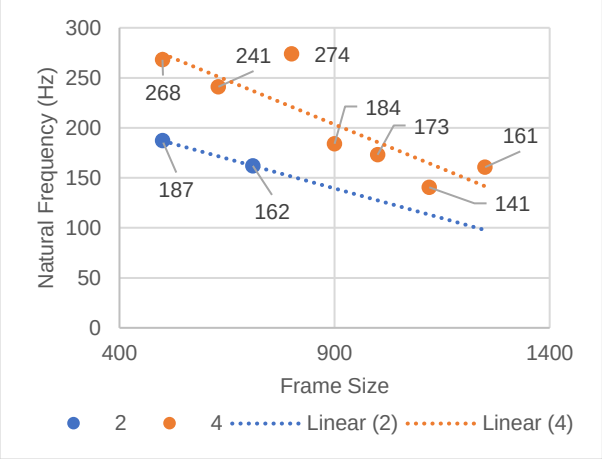

Figure 19 – Summary of natural frequencies for 02 and 04 poles

Out of the range of IEC 60034 the EWRT is recommended for 02 pole and for 04 pole with the frame size above 800 mm and 1000 mm, respectively. The reference is not by power but the frame size. This is because for the same frame, depending on the length of the stator core and voltage, there can be a wide range in power.

It is important to emphasize that the fixation of end-winding vary according to each manufactory. In this way, for the first supply of machine of two and four poles the EWRT is recommended.

VII. REFERENCES

[1] Letal, B. J., Satmoko, B., Manik, N., & Stone, G. (2020). *Stator End-Winding Vibration in Two-Pole Machines*. *December*.

[2] IEC 60505:2011 Evaluation and qualification of electrical insulation systems

[3] EC TS 60034-32:2016 Rotating electrical machines - Part 32: Measurement of stator end-winding vibration at form-wound windings

VI. VITA

Lucas Selonke Klaas received his B.S. and M.S. degree in mechanical engineering and science and engineering of materials from the State University of Santa Catarina, Brazil, in 2007 and 2013, respectively. Currently, he is doing a doctorate in electrical engineering. His research interest is bearingless motor. He is a design engineer and vibration specialist of WEG Energy since 2008. E-mail: lucask@weg.net

Fredemar Rüncos graduated in Electrical Engineering in August 1980 and in Physics in December 1980 from the Federal University of Paraná (UFPR). He has a postgraduate degree in Electrical Engineering from the Federal University of Santa Catarina (UFSC) in 1998, master's degree in electrical engineering from UFSC in 2002 and PhD also from UFSC in 2006. He started in the industry in 1968 as an apprentice in electrical machines at the company WEG, where he spent his entire professional career in the design of asynchronous machines and large synchronous machines. His activities, both in Industry and in Academic area, have always been focused on the area of Asynchronous and Synchronous Three-Phase Electrical Machines, giving him a vast experience of more than 47 years in Electrical Machines, as a Professor, Researcher, Designer and Analyst of Electrical Machines. E-mail: fredemar@weg.net

Fernando Roberto Spezia received the B.Sc. in electrical engineering from the University of the State of Santa Catarina (UDESC) in 2005. He joined WEG, Brazil, in 2006, where he has been working as an Electrical Processes and Insulation Specialist. His main areas of interest are: ageing mechanisms and reliability of insulation systems for rotating electrical machines, physics of dielectrics, dielectric materials, manufacturing processes and equipment, on-line and off-line insulation condition assessment, testing techniques, composites, and polymers. E-mail: fernandors@weg.net